Evaluation of the newly developed pocket-type dynamical double-folding potential: Systematic calculations of α-decay half-lives and nuclear charge radii*

Hai-Lan Zheng,[1,2] Da-Ming Deng,[2,†] and Zhong-Zhou Ren[1,‡]

[1]*School of Physics Science and Engineering, Tongji University, Shanghai 200092, China*
[2]*College of Physics and Optoelectronic Engineering, Shenzhen University, Shenzhen 518060, China*

The α-nucleus interaction is crucial in the description of α decay. Recently, we developed a pocket-type dynamical double-folding potential (DDFP) that effectively incorporates both the surface-medium effect and interior Pauli repulsion in the α decay [H. Zheng *et al.* ., Phys. Rev. C **109**, L011301 (2024)]. This potential results in a pocket geometry within the nuclear surface region, which is consistent with the α-clustering characteristics predicted by microscopic calculations. In this study, the accuracy of the pocket-type DDFP was validated via systematic calculations of α-decay half-lives and an extended evaluation of the nuclear charge radii of the daughter nuclei. The results demonstrate good agreement with the experimental data for both quantities, thereby confirming the reliability of the DDFP model. Compared with calculations that use α-nucleus interactions derived from conventional double-folding procedures, DDFP employs fewer adjustable parameters to achieve a more accurate description of the charge radii based on the experimental α-decay energies.

Keywords: α decay, nuclear charge radii, α-clustering effect

I. INTRODUCTION

Nucleon clustering is fundamental in the study of nuclear structures and reactions [1–4]. In particular, the clustering effect plays a crucial role in understanding cluster radioactivity and α decay in both heavy and superheavy nuclei. Although α decay has been observed in laboratories for over a century, recent experiments have directly demonstrated the formation of α clusters at the surface of heavy nuclei using $(\mathrm{p}, \mathrm{p}\alpha)$ knockout reactions [5]. However , this clustering feature in heavy nuclei has long been a key assumption in various cluster model theories of α decay, where it is attributed to the enhanced α correlation in the surface region [6–10].

Studies on few-body correlations in nuclear matter (medium) have demonstrated that the α correlation is highly sensitive to nucleon density, owing to the Pauli exclusion principle [4, 11–16]. This α correlation becomes prominent only when the medium density is below a critical threshold of approximately one-fifth the saturation density, known as the Mott density. Above this density threshold, the α correlation is suppressed owing to the antisymmetrization of the many-body wave function for the entire fermion system [12, 16].

Consequently, the formation of α clusters in a finite nucleus is confined to the nuclear surface, where nucleon density is relatively low. As the α cluster moves from the surface toward the residual daughter nucleus, it experiences increasing Pauli blocking from the surrounding nucleons (see Eq. (45) in Ref [12]). This Pauli blocking weakens the binding of the α-like quartet (α correlation), resulting in the expansion of the cluster, a phenomenon referred to as a medium effect. When the medium density exceeds the Mott density, the α correlation vanishes and the quartet transitions from a bound α-cluster state to single-nucleon states [12, 13, 16]. Therefore, α clusters rarely form in the interior of heavy nuclei.

Based on the aforementioned experimental and theoretical findings, the α cluster in the α-daughter configuration of an α emitter is expected to experience a pocket-like potential at the nuclear surface during its center-of-mass motion [12, 17–20]. Our recent study investigated the correlation between this pocket structure and the α-clustering effect [21]. We developed a pocket-type dynamical double-folding potential that incorporates both the surface-medium effect and interior Pauli repulsion for α decay. The improved α-nucleus potential results in a surface pocket geometry beyond the critical radius that marks the Mott density, thereby concentrating the α-cluster wave function at the nuclear surface beyond this radius in a self-consistent manner .

In this study, we assess the reliability of the pocket-type DDFP model further by extending the calculations of α-decay half-lives to a broader range of even-even nuclei with $60 \leq Z \leq 98$. In addition, it has been demonstrated that α-decay cluster models with double-folding potentials can be applied to estimate the nuclear charge radii [22–24]. As an additional test of the effectiveness of the DDFP model, we tentatively calculated the root-mean-square (RMS) charge radius of the daughter nucleus and compared the results with those of previous studies.

The remainder of this paper is organized as follows. In Sec. II, we present the theoretical framework of the pocket-type DDFP and half-life calculations. In Sec. III, we present the results and discuss the α-nucleus potential, α-decay half-lives, and nuclear charge radii. Finally, a summary is provided in the last section.

* This work was supported by the National Natural Science Foundation of China (Grant No. 12035011, No. 11975167, No. 12175151, No. 12005139, No. 11947123), the Guangdong Major Project of Basic and Applied Basic Research (Grant No. 2021B0301030006), the Steady Support Program for Higher Education Institutions of Shenzhen (Grant No. 20200810163629001, 20200817005440001)

† Corresponding author, ddm@szu.edu.cn
‡ Corresponding author, zren@tongji.edu.cn

II. THEORETICAL FRAMEWORK

In the cluster models for α decay, the relative motion between the α cluster and daughter nucleus is described as two-body dynamics. The α cluster interacts with the daughter nucleus via the α-nucleus potential, which can be expanded as

$$V(\boldsymbol{R}) = V_{\rm N}(\boldsymbol{R}) + V_{\rm C}(\boldsymbol{R}) + \frac{L(L+1)\hbar^2}{2\mu R^2}. \quad (1)$$

In the DDFP framework [25, 26], the nuclear potential $V_{\rm N}$ and Coulomb potential $V_{\rm C}$ are constructed using a dynamical double-folding procedure.

$$V_{\rm N,C}(\boldsymbol{R}) = \int \rho_1(\boldsymbol{r_1})\,\rho_2[\boldsymbol{r_2},\rho_1(\boldsymbol{R})]\,V_{\rm N,C}(\boldsymbol{s})\,{\rm d}\boldsymbol{r_1}{\rm d}\boldsymbol{r_2}. \quad (2)$$

$\boldsymbol{r_1}$ and $\boldsymbol{r_2}$ are the intrinsic coordinates of the daughter nucleus and the α-cluster, respectively, and $\boldsymbol{s} = \boldsymbol{R} + \boldsymbol{r_2} - \boldsymbol{r_1}$ is the vector between the interacting nucleons. A notable distinction in the DDFP formalism, compared with the conventional double-folding formalism, is the incorporation of the surface medium effect within the dynamical density distribution of the α cluster $\rho_2[\boldsymbol{r_2},\rho_1(\boldsymbol{R})]$,

$$\rho_2[\boldsymbol{r_2},\rho_1(\boldsymbol{R})] = \rho_{2,s}(\boldsymbol{R})\exp\{-\beta[\rho_1(\boldsymbol{R})]\,r_2^2\}. \quad (3)$$

This describes the size variation of the α-cluster at different medium densities $\rho_1(\boldsymbol{R})$ on the nuclear surface. The density-dependent width parameter β is determined by $\beta[\rho_1(\boldsymbol{R})] = \frac{0.7024}{1+\frac{45}{16\rho_{1,s}}\rho_1(\boldsymbol{R})}$, which satisfies the critical constraints on the intrinsic dynamics of the α cluster from the microscopic calculations [12]. The saturation density of the α cluster $\rho_{2,s}(\boldsymbol{R})$ is determined by normalizing the density distribution for each $\boldsymbol{R}$. The medium density is approximated by the local density of the daughter nucleus, which is described by the two-parameter Fermi (2pF) distribution

$$\rho_1(\boldsymbol{r_1}) = \frac{\rho_{1,s}}{1+\exp[(r_1 - R_{1/2})/a]}, \quad (4)$$

where, a represents the diffuseness parameter and $R_{1/2}$ is the half-density radius. Based on the nuclear saturation property, the half-density radius is usually expressed as

$$R_{1/2} = r_0 A^{1/3}, \quad (5)$$

under the assumption of spherical symmetry with $r_0 = 1.070$ fm. However, studies on nuclear density distributions and nuclear surface properties have indicated that the radius parameter r_0 for heavy nuclei is slightly larger than that for light nuclei [27, 28]. Based on this, we fit the theoretical half-density radius, which was derived from calculations using the SkM* functional in Ref. [28]. The fitting yielded $r_0 = 1.125$ fm for heavy nuclei with $Z = 58-96$. The diffuseness parameter a of each daughter nucleus was determined in the subsequent calculation, whereas the saturation density $\rho_{1,s}$ was determined by normalizing Eq. (4).

The effective nucleon-nucleon (NN) interaction $V_{\rm N}$ is crucial for double-folding potentials because it significantly influences the geometry of the derived potential. It was observed that strong repulsive behavior for $V_{\rm N}$ in the region of large-density overlaps is essential for simulating the Pauli blocking experienced by the α cluster, which leads to a pocket-type potential [17, 21, 29]. Here, we adopt the density-dependent Migdal NN interaction [21, 30, 31]

$$V_{\rm N}(\rho_1,\rho_2,\boldsymbol{s}) = C_0\{F_{\rm in}x(\rho_1,\rho_2) + F_{\rm ex}[1-x(\rho_1,\rho_2)]\} \times \delta(\boldsymbol{s}), \quad (6)$$

with the interaction parameters $C_0 = 300$ MeV fm^3, $F_{\rm in} = 0.09$ being well justified by fitting the experimentally measured nuclear properties [27, 30], and parameter $F_{\rm ex} = -3.82$ tuned to reproduce the experimental decay energy of ^{210}Po, and the diffuseness parameter of the daughter nucleus ^{206}Pb derived from elastic electron scattering [32]. The strength of the interaction between touching nucleons is determined by the density-dependent term $x(\rho_1,\rho_2)$ which is given by

$$x(\rho_1,\rho_2) = \frac{\rho_1(\boldsymbol{r_1}) + \rho_2(\boldsymbol{r_2},\boldsymbol{R})}{\rho_{00}(\boldsymbol{R})}, \qquad \rho_{00}(\boldsymbol{R}) = \frac{\rho_{1,s} + \rho_{2,s}(\boldsymbol{R})}{2}. \quad (7)$$

It should be noted that the medium effect also influences the NN interaction through the density-dependent term $x(\rho_1,\rho_2)$ because both ρ_2 and ρ_{00} depend on $\boldsymbol{R}$.

The α-decay width was calculated using a two-potential approach (TPA) [33]. Within the TPA framework, the tunneling problem is divided into bound-state and scattering-state problems. The decay width is expressed in terms of the bound-state wave function $\phi(R)$ and the regular scattering wave function $\chi_l(kR)$:

$$\Gamma = \frac{\hbar^2}{\mu k}|\phi(\bar{R})[\alpha\chi_l(\bar{R}) + \chi_l'(\bar{R})]|^2. \quad (8)$$

Here, $k = \sqrt{2\mu Q_\alpha/\hbar^2}$, $\alpha = \sqrt{2\mu(V(\bar{R}) - Q_\alpha)/\hbar^2}$, and $\bar{R}$ denotes the separation radius selected as the midpoint between the top of the Coulomb barrier and the outer classical turning point. The bound-state wave function $\phi(R)$ was numerically computed by solving the Schrödinger equation within the inner potential defined in TPA [33]. Regarding the scattering term, $\chi_l(R)$ can be approximated using the regular Coulomb wave function $F_l(R)$. The eigenvalue of the bound state was adjusted to match the decay energy Q_α by varying the diffuseness parameter a of the daughter nucleus.

Finally, the decay half-life was calculated using the following equation:

$$T_{1/2} = \frac{\hbar\ln 2}{P_\alpha\Gamma}, \quad (9)$$

where P_α is the α preformation factor that represents the probability of formation of an α cluster inside the parent nucleus.

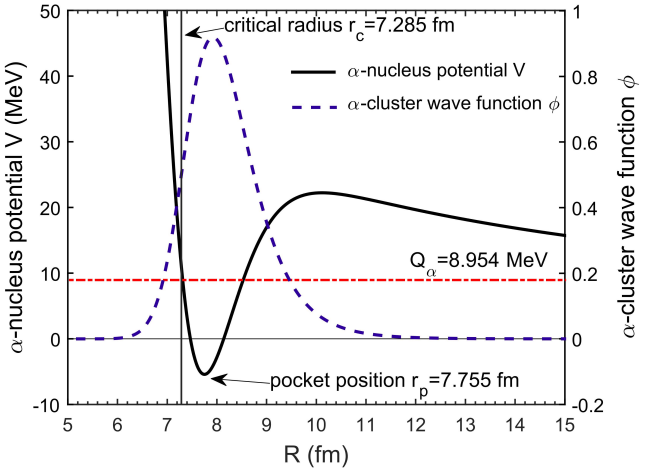

Fig. 1. (Color online) Pocket-type dynamical double-folding potential (black solid curve) and the corresponding α-cluster wave function (blue dashed curve) as a function of internuclear distance R for the $^{208}\mathrm{Pb}+\alpha$ system (ground-state to ground-state α decay in ^{212}Po). The horizontal red dotted-dashed line denotes the α decay energy Q_α. The pocket position r_p referring to the minimum of the potential is marked. The vertical black thin line denotes the critical radius r_c indicating the Mott density at the nuclear surface.

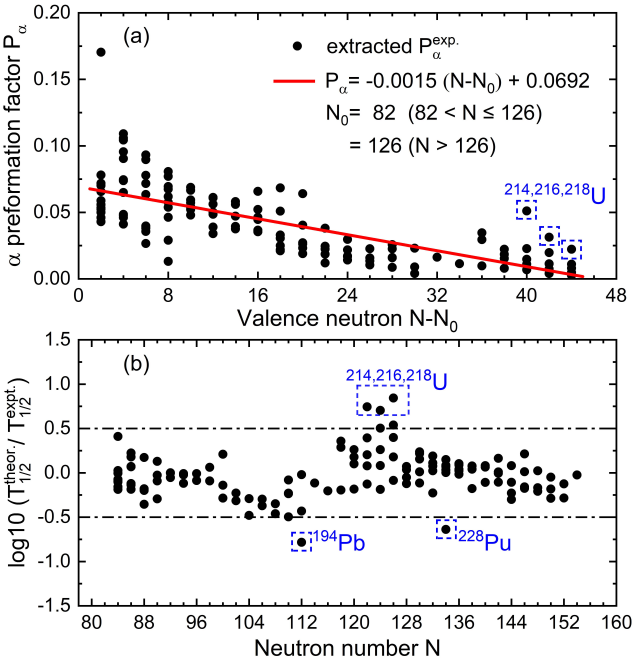

Fig. 2. (a) (Color online) Extracted α preformation factor $P_\alpha^{\mathrm{exp.}}$ (black circles) as a function of the number of valence neutrons $N-N_0$, with N_0 being the neutron magic number. The P_α generally decreases with increasing the number of valence neutrons, which can be approximated by a linear fit (red line). (b) The logarithmic deviation between the theoretical and experimental α-decay half-lives as a function of the neutron number of the parent nucleus. The dashed-dotted lines mark the range from -0.5 to 0.5. The blue dashed boxes mark the data points of ^{194}Pb, ^{214,216,218}U, and ^{228}Pu which deviate relatively far from the experimental data.

III. RESULTS AND DISCUSSIONS

A. The pocket-type DDFP and the α-decay half-life calculations

As mentioned in Sec. I, α-clustering primarily occurs at the surface of heavy nuclei where the nucleon density is below the Mott density. This is illustrated by the pocket-type DDFP, as depicted in Fig. 1. A pocket-like geometry is formed in the surface region beyond the critical radius r_c which corresponds to the Mott density. This feature enables the formation of a quasi-bound state for the α-daughter system, and the α cluster is located at the pocket center. Conversely, within the internal region ($R < r_\mathrm{c}$), Pauli repulsion suppresses the α correlation, preventing the formation of the α-cluster state. Consequently, the strongly repulsive core in the α-nucleus potential effectively inhibits the α cluster, as illustrated by the amplitude of the α-cluster wave function. The first classical turning point is close to the critical radius r_c. This classical turning point marks the boundary of the classical forbidden region, within which the amplitude of the α-cluster wave function undergoes rapidly reduction. A comparable reduction in α-clustering is expected when the medium density surpasses the Mott density; specifically, when the cluster moves into the interior of the daughter nucleus, crossing the critical radius. Therefore, the positions of the first classical turning point and the critical radius are expected to be close to each other. Our calculations indicate that the average distance between these two positions was 0.085 fm for the 129 α emitters studied, reinforcing the universality of this phenomenon.

Utilizing this pocket-type DDFP model, we investigated the ground state-to-ground state α transitions in even-even nuclei ranging from Nd to Cf. To calculate the decay half-lives using Eq. (9), the P_α factor is required as a theoretical input. Because the P_α factor is strongly correlated with the shell structure, a precise description of P_α during the shell evolution is crucial for reliable half-life calculations. However, a direct evaluation of the exact P_α within a microscopic formalism is challenging because of the complexity of many-body problems. Alternatively, the value of P_α can be estimated phenomenologically from well-established P_α systematics derived from experimental half-lives

$$P_\alpha^{\mathrm{exp.}} = \frac{\hbar \ln 2}{T_{1/2}^{\mathrm{expt.}} \Gamma}. \tag{10}$$

For instance, a simple formula that depends on the valence nucleon number of the α emitter provides a reasonably accurate description of P_α as demonstrated in previous systematic calculations [34–38]. Figure 2 (a) shows the $P_\alpha^{\mathrm{exp.}}$ factors extracted from the experimental half-lives using Eq. (10) as a function of the valence neutron number with respect to its nearest neutron magic number, N_0. As shown, $P_\alpha^{\mathrm{exp.}}$ factor generally decreases with increasing valence neutron number until the next shell closure. This dispersion exhibits a linear correlation with the valence neutron number. Based on these systematics, we employed an N-dependent formula for the

P_α factor as the theoretical input in the half-life calculations:

$$P_\alpha = -0.0015(N - N_0) + 0.0692, \tag{11}$$

with $N_0 = 82$ for nuclei with $82 < N \leq 126$ and $N_0 = 126$ for nuclei with $N > 126$, as denoted by the red line in Fig. 2 (a). This input P_α formula is different from that used in our previous work, which was based on a Heaviside step function formalism [21]. This is because the previous approach was intended to describe the abrupt change in P_α near the shell closure. The present valence-nucleon-dependent formula is more appropriate for describing the systematic behavior of P_α factor in both the closed-shell and open-shell regions.

In Fig. 2 (b), the deviations between the theoretical and experimental half-lives are plotted (denoted by black circles) on a logarithmic scale as a function of the neutron number of the parent nucleus. The agreement between the theoretical and experimental results was systematically evaluated using the average deviation, defined as $\sigma = \frac{1}{N}\sum_{i=1}^{N} |\log_{10} T^{\text{theor.}}_{1/2,i} - \log_{10} T^{\text{expt.}}_{1/2,i}|$. We obtained $\sigma = 0.1820$ for the 129 even-even nuclei investigated in this study. This result corresponds to an average factor $S = 10^\sigma = 1.521$ between the theoretical and experimental half-lives, which is slightly larger than $S = 1.475$ obtained from our previous calculation [21]. Relatively large deviations were observed for the isotopes ^{214,216,218}U, as shown in Fig. 2. These deviations are primarily due to the limitation of the N-dependent formula for P_α [Eq. (11)], which cannot adequately describe the P_α behavior during the proton shell evolution [34, 35]. The input P_α for uranium isotopes that lie farther from the proton shell at $Z = 82$ is underestimated compared with that of the extracted $P^{\text{exp.}}_\alpha$, as illustrated in Fig. 2 (a). Hence, a more refined P_α that considers both the neutron and proton shell evolution would likely improve the agreement in the half-life calculations. Furthermore, large deviations were observed for ^{194}Pb and ^{228}Pu. The deviation in ^{194}Pb is likely due to its extremely small α-branching ratio $[(7.3\pm2.9)\times10^{-6}\%]$ with relatively large uncertainty [39], while the deviation in ^{228}Pu stems primarily from the uncertainty in the measured half-life, which is $1.1^{+2.0}_{-0.5}$ s [40]. Nevertheless, as an extended calculation of our previous study [21], the present result further validate the reliability and accuracy of the pocket-type DDFP in describing the α-decay half-lives.

In addition to the ground-state-to-ground-state α decay discussed above, testing the performance of the proposed model in estimating the α-decay half-lives between the excited states would be valuable. For instance, we calculated the half-life of the favored α transition from the first isomeric state of ^{193}Po ($I^\pi = 13/2^+$) to that of ^{189}Pb ($I^\pi = 13/2^+$). The theoretical result is $T^{\text{theor.}}_{1/2} = 9.53 \times 10^{-2}$ s with P_α estimated using Eq. (11). This value is in close agreement with that reported in previous theoretical studies [41, 42]. Our result is smaller than the experimentally measured half-life $T^{\text{expt.}}_{1/2} = 2.47 \times 10^{-1}$ s by a factor of 2.6, which is acceptable particularly considering that P_α of odd-A nuclei are usually smaller than that of even-even nuclei due to the Pauli blocking from the unpaired nucleon [42, 43].

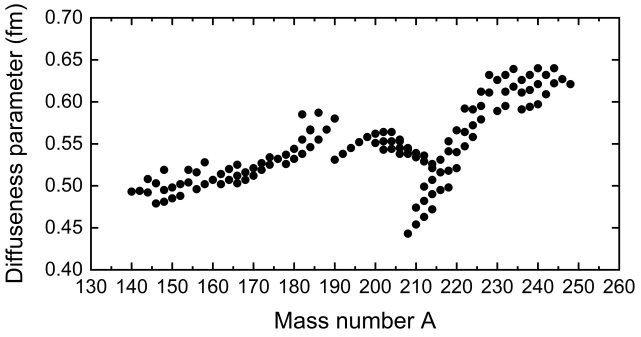

Fig. 3. (Color online) The diffuseness parameters a of the daughter nuclei, determined from the the calculations of pocket-type potentials, are plotted as a function of its mass number. The diffuseness parameters range from 0.44 fm to 0.64 fm for nuclei with $A = 140 - 248$.

B. Nuclear charge radii estimated by the pocket-type DDFP model

Within the double-folding framework, the density distribution of the daughter nucleus is involved in constructing the α-nucleus potential. Consequently, deducing the nuclear charge radius of the daughter nucleus from its density distribution is feasible once the α-nucleus potential is determined using experimental decay data. For instance, in Ref. [22, 23], the charge radii of the daughter nuclei were determined using both the experimental half-lives and decay energies within the framework of a generalized density-dependent cluster model (GDDCM). In an extension of these work, Ref. [24] improved the GDDCM (labeled GDDCM*) by considering the neutron skin structure, differences between proton and neutron density distributions, and a more refined α preformation factor. This modification provides a better description for the charge radii. To a certain extent, the accuracy of the deduced charge radii serves as an additional test of the effectiveness of the model in describing α-nucleus interactions.

As described in Sec. II, the diffuseness parameter a in the density distribution of the daughter nucleus is determined by ensuring that the pocket-type DDFP, within the TPA framework, can support a bound state with its eigenvalue matching the experimental α-decay energy. Therefore, the pocket potential embodies both α-decay dynamics and information from the decay energy. This is linked to the density distribution and the surface diffuseness property a of the daughter nucleus through a double-folding procedure. Once the value of a is determined in the calculation, we obtain not only the α-nucleus potential for half-life calculations, but also the density distribution of daughter nuclei. Therefore, the RMS charge radius of the daughter nucleus can be calculated as follows:

$$R_{\text{ch.}} \equiv \langle r^2 \rangle^{1/2} = \left[\frac{\int \rho_1(r) r^4 \, \mathrm{d}r}{\int \rho_1(r) r^2 \, \mathrm{d}r} \right]^{1/2}. \tag{12}$$

This strategy is notably simpler than previous cluster models, which require the experimental decay energy, half-life, and

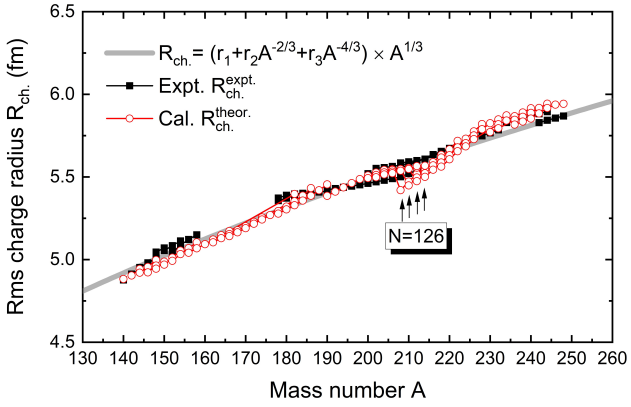

Fig. 4. (Color online) Theoretical charge radii calculated using Eq. (12) (open circles) compared with experimental data (dark squares) as a function of mass number. The grey line represents the empirical relationship between nuclear radius and mass number [Eq. (13)]. Arrows indicate the shell closure at $N = 126$ for isotopic chains of Pb, Po, Ra, and Th, where a sudden drop in calculated radii occurs due to the shell effect.

the introduction of an empirical P_α factor.

The diffuseness parameters determined using the double-folding procedure are shown in Fig. 3. The diffuseness parameters of the daughter nuclei generally fluctuate around the average value of $\bar{a} = 0.545$ fm. A clear shell effect can be observed around $A = 208$, corresponding to a neutron number approaching the $N = 126$ shell closure.

In Fig. 4, we present the calculated charge radii of the daughter nuclei with $Z = 58-96$ and the corresponding experimental values obtained from Ref. [44, 45]. The empirical relationship between the charge radius and the mass number is indicated by the gray line for reference.

$$R_{\rm ch.} = (r_1 + r_2 A^{-2/3} + r_3 A^{-4/3}) \times A^{1/3}, \qquad (13)$$

where, the parameters $r_1 = 0.9071(13)$ fm, $r_2 = 1.105(25)$ fm, and $r_3 = -0.548(34)$ fm [44]. As shown, our results align with the trend of the experimental data as well as that indicated by the empirical formula. The standard deviation of the discrepancy between the theoretical and experimental values is evaluated as $\sigma_{\rm ch.} = \left[\sum_{i=1}^{84}\left(R^{\rm theor.}_{{\rm ch.},i} - R^{\rm expt.}_{{\rm ch.},i}\right)^2/84\right]^{1/2}$ yielding a value $\sigma_{\rm ch.} = 0.0420$ fm, which was comparable to the empirical results calculated using Eq. (13). However, a notable discrepancy is observed at $A = 208-214$, where the calculated radii indicate an abrupt decrease, whereas the corresponding experimental radii vary more smoothly. This abrupt variation is related to the $N = 126$ shell effect, which significantly affects the neutron density distribution in the daughter nucleus [46]. The resulting variation in the neutron distribution, in turn, affects the proton distribution, which is reflected in a less pronounced kink appearing in the variation of the experimental charge radii at the neutron magic number (see Fig. 1 in Ref. [47] and Fig. 3 in Ref. [44]). However, the present DDFP formalism does not treat the proton and neutron distributions separately; because, it employs only one set of parameters, $R_{1/2}$ and a. The $N = 126$ shell effect from the decay energy is incorporated into the parameters shared by both the proton and neutron density distributions [21]. This results in the magnification of the shell effect for the proton distributions, thereby impacting the charge radii. Therefore, a separate treatment for both the proton and neutron density profiles, considering the neutron skin structure, is expected to reduce this discrepancy and provide a more accurate description of both the charge radii and α-decay half-lives [48, 49].

Table 1. Standard deviation $\sigma_{\rm ch.}$ between $R^{\rm expt.}_{\rm ch.}$ and $R^{\rm theor.}_{\rm ch.}$ from different cluster models for even-even nuclei with $Z = 58-96$. The first column shows the models in use. The second column lists the number of nuclei involved in the evaluation of $\sigma_{\rm ch.}$. The last column shows the values of $\sigma_{\rm ch.}$.

Cluster models	Data numbers	$\sigma_{\rm ch.}$ (fm)
Pocket-type DDFP	84	0.0420
GDDCM [22]	81	0.1284
GDDCM* [24]	83	0.0900

In addition, the charge radii of the pocket-type DDFP and previous GDDCMs can be quantitatively compared [22, 24]. Table 1 lists the standard deviations $\sigma_{\rm ch.}$ of the nuclear charge radii for these models compared with the experimental data from [44, 45]. Notably, although the DDFP relies solely on the experimental decay energy and reduces one free parameter by avoiding the input of empirical P_α, it yields a more accurate description for the charge radii. Specifically, the standard deviation is reduced by 67.3% compared to GDDCM and by 53.3% compared to GDDCM*. This significant improvement underscores the significance of the α-clustering features in the mechanism of α decay, particularly the medium effect and the strong Pauli repulsion, which make the pocket-type DDFP a more realistic description of the involved α-nucleus interaction.

Having determined the charge radii, it is instructive to

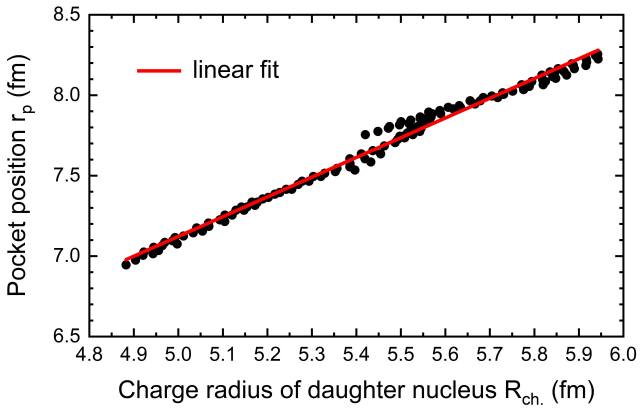

Fig. 5. (Color online) Positions of the pocket structures in the α-nucleus potentials as functions of the theoretical charge radii of daughter nuclei. These two quantities show an evident linear correlation with the correlation coefficient up to 0.9885, which emphasizes the α-clustering feature of the α-nucleus potential.

investigate the correlation between the charge radii of the daughter nuclei and the pocket positions $r_{\rm p}$ of the α-nucleus potentials (see Figs. 1 for ^{212}Po). As seen in Fig. 5, the pocket position is linearly correlated with the charge radius of the daughter nucleus with a correlation coefficient of 0.9885. This finding was expected, because both quantities are related to the spatial extent of the density distribution of the daughter nucleus. The pocket position corresponds to the region where the α cluster is most likely to form, and is located at the nuclear surface with a nucleon density below $1/5$ of the saturation density. If the daughter nucleus had a broader density distribution, the pocket position would shift away from the core region, which would yield a larger charge radius. Therefore, the correlation between these quantities embodies the α-clustering feature of the pocket-type potential.

In addition to the α-decay models, theoretical approaches based on mean-field models have proven to be very effective in describing nuclear structural properties, including nuclear charge radii [46, 50–57]. For instance, the deformed relativistic Hartree–Bogoliubov method accurately reproduced the charge radii of 369 even-even nuclei with $Z = 8-96$, achieving a standard deviation $\sigma_{\rm ch.} = 0.032$ fm [46], which was significantly more accurate than the results presented in Table 1. This higher accuracy is expected because mean-field models typically have more fitting parameters than α-decay models. For instance, the present calculation uses only three free parameters (r_0, a, and $F_{\rm ex}$) to achieve reasonable descriptions of both α-decay half-life and the nuclear charge radius. The calculation was simpler and the accuracy was acceptable as a comparative reference. Specifically, the present pocket-type DDFP approach offers a more accessible means of calculation, provided the experimental decay energy data are available.

IV. SUMMARY

This study employed the pocket-type dynamical double-folding α-nucleus potential (DDFP) to calculate the α-decay half-lives for 129 even-even nuclei with $Z = 60-98$. The experimental half-lives were accurately reproduced, with an average discrepancy factor of 1.521, thereby demonstrating the precision of DDFP in describing α decay. Moreover, the determination of the DDFP enabled the estimation of the nuclear charge radii from the density distributions of the daughter nuclei. As an improvement over our previous cluster models, DDFP achieves a more accurate description of charge radii with fewer parameters and relies soley on the experimental α-decay energies. The standard deviation between the theoretical and experimental charge radii for 84 even-even nuclei with $Z = 58-96$ is 0.0420 fm, which represents a 53.3% reduction relative to previous calculations [24], although it remains larger than that of some microscopic calculations based on mean-field theories. Notably, the present model provides an approach for estimating the nuclear charge radius from α-decay data, provided that the experimental decay energy is available. It is expected that the accuracy of DDFP can be further improved by refining the density distribution of the daughter nuclei, such as including the differences between the proton and neutron density distributions and considering nuclear deformations. Overall, the strong agreement between theoretical and experimental charge radii serves as further validation of the accuracy of DDFP for α-decay calculations.

[1] K. Ikeda, N. Takigawa, H. Horiuchi, The systematic structure-change into the molecule-like structures in the self-conjugate $4n$ nuclei. Prog. Theor. Phys. Suppl. **E68**, 464–475 (1968). http://dx.doi.org/10.1143/PTPS.E68.464

[2] Z. Ren, B. Zhou, Alpha-clustering effects in heavy nuclei. Front. Phys. **13**, 132110 (2018). https://doi.org/10.1007/s11467-018-0846-3

[3] Y.G. Ma, Effects of α-clustering structure on nuclear reaction and relativistic heavy-ion collisions. Nucl. Tech. **46**, 080001 (2023). https://dx.doi.org/10.11889/j.0253-3219.2023.hjs.46.080001

[4] R. Wang, Y.G. Ma, L.W. Chen et al., Kinetic approach of light-nuclei production in intermediate-energy heavy-ion collisions. Phys. Rev. C **108**, L031601 (2023). http://dx.doi.org/10.1103/PhysRevC.108.L031601

[5] J. Tanaka, Z. Yang, S. Typel et al., Formation of α clusters in dilute neutron-rich matter. Science **371**, 260–264 (2021). http://dx.doi.org/10.1126/science.abe4688

[6] K. Varga, R.G. Lovas, R.J. Liotta, Absolute alpha decay width of ^{212}Po in a combined shell and cluster model. Phys. Rev. Lett. **69**, 37–40 (1992). http://dx.doi.org/10.1103/PhysRevLett.69.37

[7] K. Varga, R. Lovas, R. Liotta, Cluster-configuration shell model for alpha decay. Nucl. Phys. A **550**, 421–452 . https://doi.org/10.1016/0375-9474(92)90017-E

[8] D.S. Delion, J. Suhonen, Microscopic description of α-like resonances. Phys. Rev. C **61**, 024304 (2000). http://dx.doi.org/10.1103/PhysRevC.61.024304

[9] D.S. Delion, R.J. Liotta, Shell-model representation to describe α emission. Phys. Rev. C **87**, 041302 (2013). http://dx.doi.org/10.1103/PhysRevC.87.041302

[10] C. Qi, Alpha decay as a probe for the structure of neutron-deficient nuclei. Rev. Phys. **1**, 77–89 (2016). https://doi.org/10.1016/j.revip.2016.05.001

[11] K. Hagel, R. Wada, L. Qin et al., Experimental determination of in-medium cluster binding energies and mott points in nuclear matter. Phys. Rev. Lett. **108**, 062702 (2012). http://dx.doi.org/10.1103/PhysRevLett.108.062702

[12] G. Röpke, P. Schuck, Y. Funaki et al., Nuclear clusters bound to doubly magic nuclei: The case of ^{212}Po. Phys. Rev. C **90**, 034304 (2014). http://dx.doi.org/10.1103/PhysRevC.90.034304

[13] G. Röpke, A. Schnell, P. Schuck et al., Four-particle condensate in strongly coupled fermion systems. Phys. Rev. Lett. **80**, 3177–3180 (1998). http://dx.doi.org/10.1103/PhysRevLett.80.3177

[14] G. Röpke, Light nuclei quasiparticle energy shifts in hot and dense nuclear matter. Phys. Rev. C **79**, 014002 (2009).

http://dx.doi.org/10.1103/PhysRevC.79.014002
[15] S. Typel, G. Röpke, T. Klähn et al., Composition and thermodynamics of nuclear matter with light clusters. Phys. Rev. C **81**, 015803 (2010). http://dx.doi.org/10.1103/PhysRevC.81.015803
[16] G. Röpke, C. Xu, B. Zhou et al., Alpha-like correlations in ^{20}Ne, comparison of quartetting wave function and THSR approaches. Eur. Phys. J. A **60**, 89 (2024). http://dx.doi.org/10.1140/epja/s10050-024-01305-7
[17] W.M. Seif, A.M.H. Abdelhady, A. Adel, Improved nucleus–nucleus folding potential with a repulsive core due to the change of intrinsic kinetic energy. J. Phys. G: Nucl. Part. Phys. **45**, 115101 (2018). http://dx.doi.org/10.1088/1361-6471/aae3d4
[18] D.S. Delion, A. Dumitrescu, V.V. Baran, Theoretical investigation of α-like quasimolecules in heavy nuclei. Phys. Rev. C **97**, 064303 (2018). http://dx.doi.org/10.1103/PhysRevC.97.064303
[19] A. Dumitrescu, D.S. Delion, Cluster mean-field description of α emission. Phys. Rev. C **107**, 024302 (2023). http://dx.doi.org/10.1103/PhysRevC.107.024302
[20] A. Delion, D.S.and Dumitrescu, Alpha-clustering and related phenomena in medium and heavy nuclei. Eur. Phys. J. A **59**, 210 (2023). http://dx.doi.org/10.1140/epja/s10050-023-01105-5
[21] H. Zheng, D. Deng, Z. Ren, α clustering from the formation of a pocket structure in the α-nucleus potential. Phys. Rev. C **109**, L011301 (2024). http://dx.doi.org/10.1103/PhysRevC.109.L011301
[22] D. Ni, Z. Ren, T. Dong et al., Nuclear charge radii of heavy and superheavy nuclei from the experimental α-decay energies and half-lives. Phys. Rev. C **87**, 024310 (2013). http://dx.doi.org/10.1103/PhysRevC.87.024310
[23] Y. Qian, Z. Ren, D. Ni, Tentative probe into the nuclear charge radii of superheavy odd-mass and odd-odd nuclei. Phys. Rev. C **89**, 024318 (2014). http://dx.doi.org/10.1103/PhysRevC.89.024318
[24] Y. Qian, Z. Ren, Improved evaluation of nuclear charge radii for superheavy nuclei. J. Phys. G: Nucl. Part. Phys. **45**, 085103 (2018). http://dx.doi.org/10.1088/1361-6471/aacef7
[25] D. Deng, Z. Ren, Improved double-folding α-nucleus potential by including nuclear medium effects. Phys. Rev. C **96**, 064306 (2017). http://dx.doi.org/10.1103/PhysRevC.96.064306
[26] D. Deng, Z. Ren, N. Wang, Significant improvement of half-life calculation of α decays by considering the nuclear medium effect. Phys. Lett. B **795**, 554–560 (2019). https://doi.org/10.1016/j.physletb.2019.06.045
[27] G.G. Adamian, N.V. Antonenko, H. Lenske et al., Isotopic trends of nuclear surface properties of spherical nuclei. Phys. Rev. C **94**, 054309 (2016). http://dx.doi.org/10.1103/PhysRevC.94.054309
[28] G. Scamps, D. Lacroix, G.G. Adamian et al., Polarization of the nuclear surface in deformed nuclei. Phys. Rev. C **88**, 064327 (2013). http://dx.doi.org/10.1103/PhysRevC.88.064327
[29] V. Denisov, V. Nesterov, Effect of the pauli exclusion principle on the potential of nucleus-nucleus interaction. Phys. Atom. Nuclei **74**, 1142 (2010). https://doi.org/10.1134/S1063778810070070
[30] G.G. Adamian, N.V. Antonenko, R.V. Jolos et al., Effective nucleus-nucleus potential for calculation of potential energy of a dinuclear system. Int. J. Mod. Phys. E **5**, 191–216 (1996). http://dx.doi.org/10.1142/S0218301396000098
[31] A.B. Migdal, Quasiparticles in the theory of the nucleus. Sov. Phys. Usp. **10**, 285 (1967). http://dx.doi.org/10.1070/PU1967v010n03ABEH003247
[32] H. De Vries, C. De Jager, C. De Vries, Nuclear charge-density-distribution parameters from elastic electron scattering. At. Data Nucl. Data Tables **36**, 495–536 (1987). https://doi.org/10.1016/0092-640X(87)90013-1
[33] S.A. Gurvitz, G. Kalbermann, Decay width and the shift of a quasistationary state. Phys. Rev. Lett. **59**, 262–265 (1987). http://dx.doi.org/10.1103/PhysRevLett.59.262
[34] Z. Ren, G. Xu, Reduced alpha transfer rates in a schematic model. Phys. Rev. C **36**, 456–459 (1987). http://dx.doi.org/10.1103/PhysRevC.36.456
[35] Z. Ren, G. Xu, Shell and blocking effects in α-transfer reactions. J. Phys. G Nucl. Part. Phys. **15**, 465 (1989). http://dx.doi.org/10.1088/0954-3899/15/4/010
[36] C. Xu, Z. Ren, α-decay studies of the exotic $N = 125$, 126, and 127 isotones. Phys. Rev. C **76**, 027303 (2007). http://dx.doi.org/10.1103/PhysRevC.76.027303
[37] H.F. Zhang, G. Royer, Y.J. Wang et al., Analytic expressions for α particle preformation in heavy nuclei. Phys. Rev. C **80**, 057301 (2009). http://dx.doi.org/10.1103/PhysRevC.80.057301
[38] W.M. Seif, M. Shalaby, M.F. Alrakshy, Isospin asymmetry dependence of the α spectroscopic factor for heavy nuclei. Phys. Rev. C **84**, 064608 (2011). http://dx.doi.org/10.1103/PhysRevC.84.064608
[39] Y.A. Ellis-Akovali, K.S. Toth, H.K. Carter et al., α-decay reduced width of ^{194}Pb and low-spin levels in ^{194}Tl populated in ^{194}Pb β decay. Phys. Rev. C **36**, 1529–1539 (1987). http://dx.doi.org/10.1103/PhysRevC.36.1529
[40] K. Nishio, H. Ikezoe, S. Mitsuoka et al., Half-life of ^{228}Pu and α decay of ^{228}Np. Phys. Rev. C **68**, 064305 (2003). http://dx.doi.org/10.1103/PhysRevC.68.064305
[41] J. Dong, H. Zhang, Y. Wang et al., Alpha-decay for heavy nuclei in the ground and isomeric states. Nucl. Phys. A **832**, 198–208 (2010). https://doi.org/10.1016/j.nuclphysa.2009.10.082
[42] Y. Qian, Z. Ren, D. Ni, α-decay near the shell closure from ground and isomeric states. Nucl. Phys. A **866**, 1–15 (2011). https://doi.org/10.1016/j.nuclphysa.2011.07.002
[43] D. Deng, Z. Ren, α preformation factors of medium-mass nuclei and the structural effects in the region of crossing the $Z = 82$ shell. Phys. Rev. C **93**, 044326 (2016). http://dx.doi.org/10.1103/PhysRevC.93.044326
[44] I. Angeli, K. Marinova, Table of experimental nuclear ground state charge radii: An update. At. Data Nucl. Data Tables **99**, 69–95 (2013). https://doi.org/10.1016/j.adt.2011.12.006
[45] T. Li, Y. Luo, N. Wang, Compilation of recent nuclear ground state charge radius measurements and tests for models. At. Data Nucl. Data Tables **140**, 101440 (2021). https://doi.org/10.1016/j.adt.2021.101440
[46] K. Zhang, M.K. Cheoun, Y.B. Choi et al., Nuclear mass table in deformed relativistic hartree–bogoliubov theory in continuum, i: Even–even nuclei. At. Data Nucl. Data Tables **144**, 101488 (2022). https://doi.org/10.1016/j.adt.2022.101488
[47] P.M. Goddard, P.D. Stevenson, A. Rios, Charge radius isotope shift across the N=126 shell gap. Phys. Rev. Lett. **110**, 032503 (2013). http://dx.doi.org/10.1103/PhysRevLett.110.032503
[48] Z. Wang, Z. Ren, Predictions of the decay properties of the superheavy nuclei ^{293,294}119 and ^{294,295}120. Nucl. Tech. **46**, 080011 (2023). http://dx.doi.org/10.11889/j.0253-3219.2023.hjs.46.080011

[49] D. Fang, Neutron skin thickness and its effects in nuclear reactions. Nucl. Tech. **46**, 080016 (2023). http://dx.doi.org/10.11889/j.0253-3219.2023.hjs.46.080016
[50] S. Goriely, S. Hilaire, M. Girod et al., First gogny-hartree-fock-bogoliubov nuclear mass model. Phys. Rev. Lett. **102**, 242501 (2009). http://dx.doi.org/10.1103/PhysRevLett.102.242501
[51] E.E. Saperstein, S.V. Tolokonnikov, consistent theory of finite fermi systems and radii of nuclei. Phys. Atom. Nuclei **74**, 1277 (2011). https://doi.org/10.1134/S1063778811090109
[52] R. An, X. Dong, L. Cao et al., Local variations of charge radii for nuclei with even Z from 84 to 120. Commun. Theor. Phys. **75**, 035301 (2023). http://dx.doi.org/10.1088/1572-9494/acb58b
[53] L. Wang, J. Lyu, J. Liu et al., Analysis of parity-violating electron scattering on deformed nuclei. Phys. Rev. C **109**, 064303 (2024). http://dx.doi.org/10.1103/PhysRevC.109.064303
[54] R. An, X. Jiang, N. Tang et al., Improved description of nuclear charge radii: Global trends beyond $N = 28$ shell closure. Phys. Rev. C **109**, 064302 (2024). http://dx.doi.org/10.1103/PhysRevC.109.064302
[55] Y.B. Choi, C.H. Lee, M.H. Mun et al., α-decay half-lives for even-even isotopes of W to U. Phys. Rev. C **109**, 054310 (2024). http://dx.doi.org/10.1103/PhysRevC.109.054310
[56] S. Elhatisari, L. Bovermann, Y.Z. Ma et al., Wavefunction matching for solving quantum many-body problems. Nature (London) **630**, 59 – 63 (2024). https://doi.org/10.1038/s41586-024-07422-z
[57] X. Sun, S. Zhou, Deformed halo nuclei and shape decoupling effects. Nucl. Tech. **46**, 080015 (2023). https://dx.doi.org/10.11889/j.0253-3219.2023.hjs.46.080015